ENVIRONMETRICS
Environmetrics (2010)
Published online in Wiley InterScience
(www.interscience.wiley.com) DOI: 10.1002/env.1058

Hierarchical dynamic modeling of outbreaks of mountain pine beetle using partial differential equations

Yanbing Zheng[1]*,† and Brian H. Aukema[2,3,4]

[1]*Department of Statistics, University of Kentucky, Lexington, KY 40536-0001, U.S.A.*
[2]*Canadian Forest Service, Natural Resources Canada, Prince George, BC, Canada*
[3]*Ecosystem Science and Management Program, University of Northern British Columbia, Prince George, BC, Canada*
[4]*Department of Entomology, University of Minnesota, St. Paul, MN*

SUMMARY

In this article, we develop spatial–temporal generalized linear mixed models for spatial–temporal binary data observed on a spatial lattice and repeatedly over discrete time points. To account for spatial and temporal dependence, we introduce a spatial–temporal random effect in the link function and model by a diffusion–convection dynamic model. We propose a Bayesian hierarchical model for statistical inference and devise Markov chain Monte Carlo algorithms for computation. We illustrate the methodology by an example of outbreaks of mountain pine beetle on the Chilcotin Plateau of British Columbia, Canada. We examine the effect of environmental factors while accounting for the potential spatial and temporal dependence. Copyright © 2010 John Wiley & Sons, Ltd.

KEY WORDS: Dendroctonus ponderosae; generalized linear mixed model; mountain pine beetle; partial differential equation; spatial-temporal process

1. INTRODUCTION

Outbreaks of mountain pine beetle *Dendroctonus ponderosae* Hopkins (Coleoptera: Scolytidae; alt. Curculionidae: Scolytinae) (MPB) have caused landscape-level mortality to mature trees in pine forests in western North America over the past century (Campbell *et al*., 2007; Raffa *et al*., 2008). A current outbreak in British Columbia and Alberta, Canada, now covers an area approximately 14 million hectare in size. This outbreak is an order of magnitude larger in area and severity than all previous outbreaks recorded in these two provinces, which makes MPB the second most important natural disturbance agent after fire in these forests (Kurz *et al*., 2008). Many factors influence the magnitude, propagation, and severity of outbreaks. One key environmental factor is temperature that mediates key life history traits, such as overwintering survival and summer dispersal to find new trees.

For modeling binary lattice data (here presence or absence of outbreak), an autologistic regression model is a popular and powerful tool and has been extended to spatial–temporal settings in recent years (e.g., Zhu *et al*., 2005; Zhu *et al*., 2008). In a spatial–temporal autologistic model, the response variable is

*Correspondence to: Yanbing Zheng, Department of Statistics, University of Kentucky.
†E-mail: yanbing.zheng@uky.edu

Received 31 October 2008
Accepted 6 May 2010

autoregressed to reflect the possible spatial–temporal dependence in the data. However, the normalizing constant in the likelihood function of the autologistic model is intractable and imposes computational challenges. Furthermore, the type of spatial–temporal dependence that can be featured is somewhat limited. Recently, Hooten and Wikle (2007) proposed a class of dynamic models for binary data based on a probabilitistic cellular automation approach. Instead of modeling the transformed probability of presence or absence, the dynamic model is constructed based on the untransformed probability directly. See Royle and Dorazio (2008) for a review of dynamic modeling of binary data.

Here we consider a spatial–temporal generalized linear mixed model (GLMM) as an alternative approach to modeling spatial–temporal binary data, which is an extension of the traditional GLMMs. A GLMM assumes that, conditional on random effects, the response variables are independent and can be formulated in a similar manner as the generalized linear models with explanatory variables and random effects (e.g., McCullagh and Nelder, 1989). Diggle *et al*. (1998) proposed a spatial GLMM to model spatial dependence for spatial data that are not necessarily Gaussian. In recent years, there has been a growing literature on the extension of the spatial GLMM to the space–time domain with spatial–temporal variation structure imposed on the random effects (e.g., Banerjee *et al*., 2004; Clark, 2007). Cressie and Huang (1999) and Gneiting (2002) defined several classes of valid spatial–temporal covariance structures. However, the resulting high dimensionality can prohibit its implementation in the context of GLMM. Alternatively, hierarchical spatial–temporal dynamic models are appealing because of their flexibility to accommodate multiple data sources with errors and contend with challenges such as differing resolutions in space and time and complicated dependence structures (e.g., Wikle *et al*., 2001). For example, Wikle (2003) and Hooten and Wikle (2008) used hierarchical spatial–temporal dynamic models for the analysis of spatial–temporal Poisson counts in a study of the spread of invasive species across space and over time.

In this article, we develop spatial–temporal GLMM for spatial–temporal binary data. We utilize the idea of hierarchical spatial–temporal dynamic models to account for spatial and temporal dependence, as well as interaction between space and time. We study the efficiency of incorporating PDE-based dynamics under the GLMM framework for binary data. The rest of the article is organized as follows. In Section 2, we describe the mountain pine beetle (MPB) data. In Section 3, we introduce the spatial–temporal GLMM and derive Markov chain Monte Carlo (MCMC) algorithms for Bayesian inference. A simulation study and the analysis results for the MPB example are presented in Section 4, followed by a discussion in Section 5.

2. DESCRIPTION OF THE MOUNTAIN PINE BEETLE DATA

MPB is an eruptive insect that intermittently kills mature pine trees over large areas. During outbreaks, insects colonize trees via pheromone-mediated mass attacks that, in concert with vectored fungi, exhaust host defenses. Insects must kill their host trees to reproduce in outbreak conditions. Their life cycle typically takes 1 year in western Canada. Spatially-explicit impacts of mountain pine beetle are typically estimated from annual aerial surveys, as fading crowns in areas of dying trees become visually apparent and can be mapped and digitized in a GIS.

Specifically, we examine the outbreak of MPB on the Chilcotin Plateau in British Columbia, Canada, from its endemic beginnings through the collapse period (1972–1986). During the study, a grid of 469 cells averaging 12×12 km in size is laid over the study area (see Figure 1). For each cell, mortality of lodgepole pines due to MPB was estimated from aerial survey maps of the Forest Insect and Disease Survey (FIDS) performed by the Canadian Forest Service. After correcting for survey bias, values for

DOI: 10.1002/env

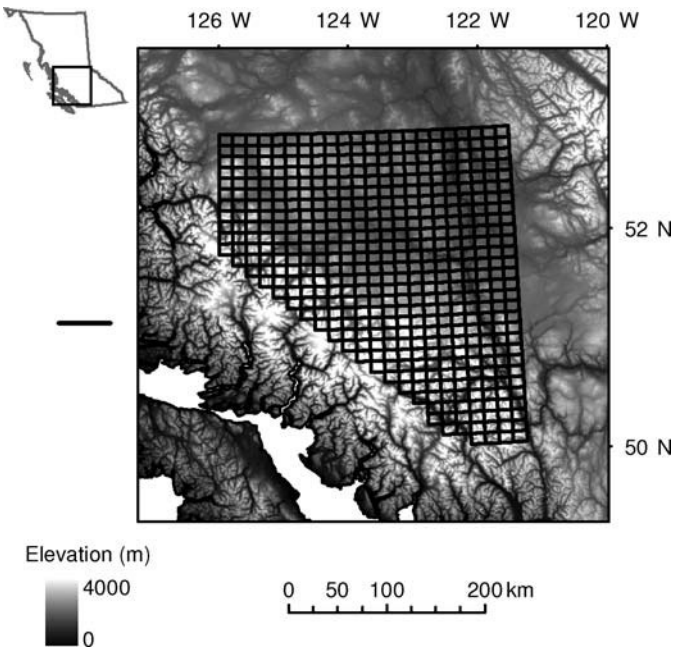

Figure 1. Digital elevation map of lower British Columbia, Canada superimposed by the grid of study area over the Chilcotin Plateau

each cell were converted to presence/absence of outbreak populations of MPB. Figure 2 is a time-series map of the outbreak from 1972 to 1986. The proportion of cells with MPB outbreak activity increased steadily throughout the 1970s, and the overall outbreak collapsed by 1986.

Many environmental factors affect the reproductive success of MPB. As in Zhu *et al*. (2008), we focus on three environmental factors: the number of cold days below -40°C, mean August temperature, and mean elevation in a cell. Development of MPBs is highly temperature dependent. Winter temperatures down to -40°C or lower for a few days is lethal to overwintering larvae and may effectively reduce population size (Wygant, 1940). Emergence of new MPB is also temperature dependent, as development from larvae through adult is governed by critical temperature thresholds that ensure synchronous emergence necessary to attack new trees *en masse* (Powell *et al*., 2000). Emergence may begin as early as July and continue through September. Previous research has determined that August temperatures may be a good indicator of beetle success (Safranyik *et al*., 1975), as warm temperatures facilitate flight and beetle establishment and cool temperatures deter infestation from spreading to adjacent areas. In addition, elevation may be a useful proxy for the distribution of host trees (e.g., Aukema *et al*., 2008), as lodgepole pines do not grow as well at high elevation over our study area.

Both short- and long-distance dispersal also affect MPB distribution. Within a forest, MPBs may fly toward a source of attractant pheromones (Safranyik *et al*., 1992). A proportion of beetles may also be captured by advective currents and be transported above the forest canopy tens or even hundreds of kilometers. Hence, diffusion and convection patterns characteristic of mesoscale atmospheric transport may ultimately affect MPB distributions on the landscape during outbreak conditions (Jackson *et al*., 2008).

DOI: 10.1002/env

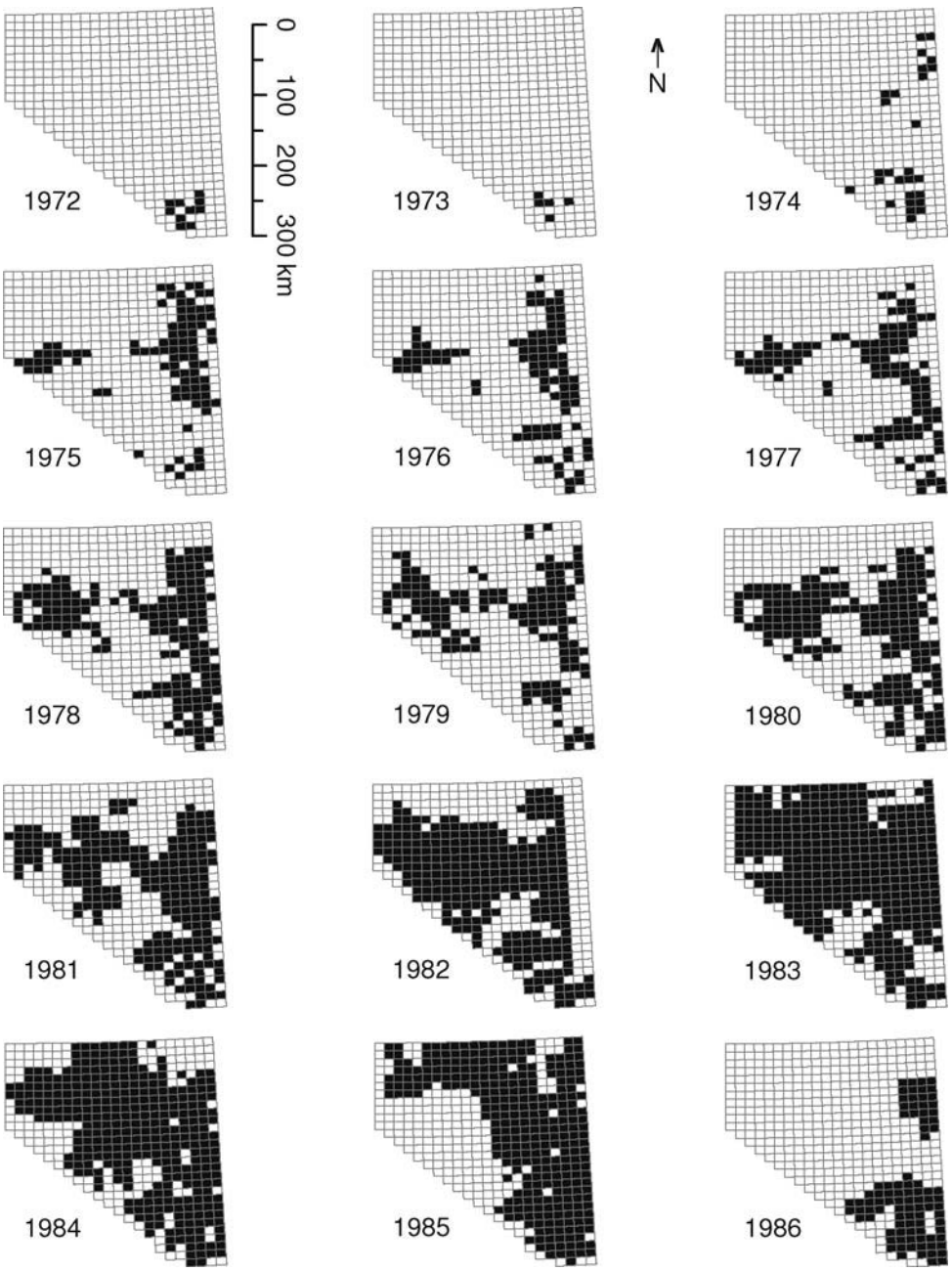

Figure 2. Maps of mountain pine beetle outbreak from 1972 to 1986. A cell is filled black if there was an outbreak and is unfilled otherwise

DOI: 10.1002/env

3. SPATIAL–TEMPORAL GENERALIZED LINEAR MIXED MODELS

With $i = 1, \ldots, n$ and $t = 1, \ldots, T$, let $Y_{i,t} = Y(\boldsymbol{s}_i, t)$ denote the binary response variable at the ith cell $\boldsymbol{s}_i$ and the tth time point, such that $Y_{i,t} = 0$ for no outbreak or 1 for outbreak. Let $\boldsymbol{Y}_t = (Y_{1,t}, \ldots, Y_{n,t})'$ denote the binary responses on the entire spatial lattice for a given time point t. Furthermore, let $X_{0,i,t} \equiv 1$ and $X_{k,i,t}$ denote the kth explanatory variable at the ith cell and the tth time point, for $k = 1, \ldots, K$, where K denotes the number of explanatory variables. In the MPB example, $K = 3$. Following Berliner (1996), we consider a three-stage hierarchical framework when specifying a spatial–temporal GLMM,

$$[\text{process, parameters}|\text{data}] \propto [\text{data}|\text{process, parameters}][\text{process}|\text{parameters}][\text{parameters}]$$

where $[\cdot]$ refers to a distribution.

3.1. Data model

Let $p_{i,t}$ denote the probability of MPB outbreak at the ith cell and tth time point and let $\boldsymbol{p}_t = (p_{1,t}, \ldots, p_{n,t})'$. Conditional on the spatial–temporal process $\{\boldsymbol{p}_t, t = 1, \ldots, T\}$, we assume that the distribution of $Y_{i,t}$ is Bernoulli and independent across space and over time,

$$[Y_{i,t}|p_{i,t}] \sim \text{Bernoulli}\,(p_{i,t})$$

for $i = 1, \ldots, n$ and $t = 1, \ldots, T$.

3.2. Process model

The logit link of the spatial–temporal process $\boldsymbol{p}_t$ is assumed to follow a linear mixed model,

$$\text{logit}(\boldsymbol{p}_t) = \sum_{k=0}^{K} \theta_k \boldsymbol{X}_{k,t} + \boldsymbol{u}_t + \boldsymbol{\epsilon}_t \tag{1}$$

where $\sum_{k=0}^{K} \theta_k \boldsymbol{X}_{k,t}$ denotes a regression on the explanatory variables $\boldsymbol{X}_{k,t} = (X_{k,1,t}, \ldots, X_{k,n,t})'$ and $\boldsymbol{u}_t = (u_{1,t}, \ldots, u_{n,t})'$ is a latent process (or random effect) explaining the remainder spatial and temporal variation after accounting for the explanatory variables to reflect dispersal. The error process $\boldsymbol{\epsilon}_t = (\epsilon_{1,t}, \ldots, \epsilon_{n,t})'$ accounts for measurement error and is assumed to be independent across space and over time with $[\boldsymbol{\epsilon}_t] \sim \text{Normal}\,(\boldsymbol{0}, \sigma_\epsilon^2 \mathbf{I})$.

A critical part of the GLMM specification is modeling the latent process $\boldsymbol{u}_t$. To feature spatial and temporal dependence, we impose a dynamic spatial–temporal model on $\boldsymbol{u}_t$,

$$\boldsymbol{u}_t = \boldsymbol{H}\boldsymbol{u}_{t-1} + \boldsymbol{\eta}_t \tag{2}$$

for $t = 1, \ldots, T$. The matrix $\boldsymbol{H}$ is referred to as a transition matrix and controls the dynamics of $\boldsymbol{u}_t$. We assume that the process $\boldsymbol{u}_t$ starts with $\boldsymbol{u}_0$ and $\boldsymbol{u}_0 \sim \text{Normal}\,(\boldsymbol{\mu}_0, \boldsymbol{\Sigma}_0)$. We will let $\boldsymbol{\mu}_0 = \boldsymbol{0}$ and $\boldsymbol{\Sigma}_0 = \sigma_0^2 \boldsymbol{I}$ with a relatively large σ_0^2 reflecting our vague belief in the initial process.

The term $\boldsymbol{\eta}_t = (\eta_{1,t}, \ldots, \eta_{n,t})'$ is to model the small-scale variation. We assume that $\boldsymbol{\eta}_t$ are spatially and temporally independent, but the model can be extended to have a spatial covariance structure (e.g.,

DOI: 10.1002/env

CAR model or variogram model) to account for the residual spatial variation. We study the possibility of incorporating different structures for $\boldsymbol{\eta}_t$ in the simulation section.

3.3. Partial differential equations model for $\boldsymbol{u}_t$

For the parameterization of transition matrix $\boldsymbol{H}$, we consider partial differential equations (PDE). There is a long history of describing insect dispersal with differential equations (see Holmes *et al*. (1994) for a review). To account for diffusion of MPB and the potential effects of advective transport, we consider a diffusion–convection equation for $\boldsymbol{u}_t$,

$$\frac{\partial u}{\partial t} = D\left(\frac{\partial^2 u}{\partial x^2} + \frac{\partial^2 u}{\partial y^2}\right) - w_x\frac{\partial u}{\partial x} - w_y\frac{\partial u}{\partial y} \tag{3}$$

where D is a diffusion coefficient representing the rate of diffusion, w_x and w_y are convection coefficients representing convection rates in the x and y directions. In the diffusion–convection model, the dispersal of insects is considered as a combination of random motion (diffusion) and directed motion (convection or advection). The magnitudes of the coefficients identify the relative strengths for the two processes. Banks *et al*. (1988) considered diffusion–convection models for studying the dispersal of female cabbage root flies. Convection occurs when insects orient toward external stimuli or are carried by the wind. That is, this spatial and temporal behavior is controlled by the interference between insects and environmental factors (de la Giroday, 2009; Okubo and Levin, 2001).

Following basic finite difference approaches, we compute the numerical solution of partial differential equations (e.g., Haberman, 1987). In particular, we apply first-order forward differences in time,

$$\frac{\partial u}{\partial t} = \frac{u_t(x, y) - u_{t-\Delta_t}(x, y)}{\Delta_t}$$

We also apply centered differences in space,

$$\begin{aligned}
\frac{\partial u}{\partial x} &= \frac{u_t(x+\Delta_x, y) - u_t(x-\Delta_x, y)}{2\Delta_x} \\
\frac{\partial u}{\partial y} &= \frac{u_t(x, y+\Delta_y) - u_t(x, y-\Delta_y)}{2\Delta_y} \\
\frac{\partial^2 u}{\partial x^2} &= \frac{u_t(x+\Delta_x, y) - 2u_t(x, y) + u_t(x-\Delta_x, y)}{\Delta_x^2} \\
\frac{\partial^2 u}{\partial y^2} &= \frac{u_t(x, y+\Delta_y) - 2u_t(x, y) + u_t(x, y-\Delta_y)}{\Delta_y^2}
\end{aligned}$$

where centered differences are valid for any time t. As a result, we have,

$$\begin{aligned}
u_t(x, y) = u_{t-\Delta_t}(x, y)&\left\{1 - 2D\left(\frac{\Delta_t}{\Delta_x^2} + \frac{\Delta_t}{\Delta_y^2}\right)\right\} \\
&+ u_{t-\Delta_t}(x+\Delta_x, y)\left(-w_x\frac{\Delta_t}{2\Delta_x} + D\frac{\Delta_t}{\Delta_x^2}\right) + u_{t-\Delta_t}(x-\Delta_x, y)\left(w_x\frac{\Delta_t}{2\Delta_x} + D\frac{\Delta_t}{\Delta_x^2}\right)
\end{aligned}$$

DOI: 10.1002/env

$$+ u_{t-\Delta_t}(x, y+\Delta_y)\left(-w_y\frac{\Delta_t}{2\Delta_y} + D\frac{\Delta_t}{\Delta_y^2}\right) + u_{t-\Delta_t}(x, y-\Delta_y)\left(w_y\frac{\Delta_t}{2\Delta_y} + D\frac{\Delta_t}{\Delta_y^2}\right)$$
$$+ \eta_t(x, y) \tag{4}$$

We assume that the spatial increments and temporal increment are $\Delta_x = \Delta_y = \Delta_t = 1$. According to our simulation study, this unit increment works reasonably well in our current framework. For high-order dynamics, smaller increments may be required to provide a good approximation to the partial different equation. We further assume that $u_t(x, y) = 0$ if cell (x, y) is not in the study domain. Thus, we have,

$$\boldsymbol{u}_t = \boldsymbol{H}(D, w_x, w_y)\boldsymbol{u}_{t-1} + \boldsymbol{\eta}_t \tag{5}$$

where the transition matrix $\boldsymbol{H}$ depends upon the diffusion and convection coefficients.

3.4. Parameter model and Bayesian inference

For statistical inference, we adopt a Bayesian hierarchical modeling framework. The Bayesian formulation of the hierarchical model is summarized by the following posterior distribution,

$$\begin{aligned} &p(\boldsymbol{p}_1, \ldots, \boldsymbol{p}_t, \boldsymbol{u}_0, \ldots, \boldsymbol{u}_T, \sigma_\epsilon^2, D, w_x, w_y, \sigma_\eta^2 | \boldsymbol{Y}_1, \ldots, \boldsymbol{Y}_T) \\ &\quad \propto \left\{\prod_{t=1}^{T} p(\boldsymbol{Y}_t|\boldsymbol{p}_t)p(\boldsymbol{p}_t|\boldsymbol{\theta}, \boldsymbol{u}_t, \sigma_\epsilon^2)\right\}\left\{\prod_{t=1}^{T} p(\boldsymbol{u}_t|\boldsymbol{u}_{t-1}, D, w_x, w_y, \sigma_\eta^2)p(\boldsymbol{u}_0)\right\} \\ &\quad \times p(\boldsymbol{\theta})p(D)p(w_x)p(w_y)p(\sigma_\epsilon^2)p(\sigma_\eta^2) \end{aligned} \tag{6}$$

where $\boldsymbol{\theta} = (\theta_0, \ldots, \theta_K)'$ denotes the vector of regression coefficients. To sample from the posterior (6), we implement a Gibbs sampler and update the parameters component-wise. Specifically, we transform $p_{i,t}$ to be $v_{i,t} = \text{logit}(p_{i,t})$ for $i = 1, \ldots, n$ and $t = 1, \ldots, T$, and sample it from a full conditional distribution by utilizing a Metropolis–Hastings (MH) procedure. Then $v_{i,t}$ is transformed back to $p_{i,t} = \exp(v_{i,t})/\{1 + \exp(v_{i,t})\}$. The latent process $\boldsymbol{u}_t$ with $t = 0, \ldots, T$ can be sampled from their full conditional distributions directly. We assume conjugate normal priors for regression coefficients $\boldsymbol{\theta}$ and diffusion and convection coefficients D, w_x and w_y and conjugate inverse-gamma priors for variance parameters σ_ϵ^2 and σ_η^2. We sample these parameters according to their full conditional distributions.

Let $\boldsymbol{Y} = (\boldsymbol{Y}_1', \ldots, \boldsymbol{Y}_T')'$. For prediction at future time points $T+1, \ldots, T+\Delta T$, we consider the posterior predictive distribution,

$$\begin{aligned} &p(\boldsymbol{Y}_{T+1}, \ldots, \boldsymbol{Y}_{T+\Delta T}|\boldsymbol{Y}) \\ &= \int \left(\prod_{\Delta t=1}^{\Delta T} p(\boldsymbol{Y}_{T+\Delta t}|\boldsymbol{p}_{T+\Delta t})\right) p(\boldsymbol{p}_{T+1} \ldots, \boldsymbol{p}_{T+\Delta T}|\boldsymbol{Y}) d\boldsymbol{p}_{T+1} \cdots d\boldsymbol{p}_{T+\Delta T} \end{aligned}$$

DOI: 10.1002/env

$$= \int \left(\prod_{\Delta t=1}^{\Delta T} p(\boldsymbol{Y}_{T+\Delta t}|\boldsymbol{p}_{T+\Delta t}) p(\boldsymbol{p}_{T+\Delta t}|\boldsymbol{\theta}, \boldsymbol{u}_{T+\Delta t}, \sigma_\epsilon^2) p(\boldsymbol{u}_{T+\Delta t}|\boldsymbol{u}_{T+\Delta t-1}, D, w_x, w_y, \sigma_\eta^2) \right)$$
$$p(\boldsymbol{u}_T, \boldsymbol{\theta}, D, w_x, w_y, \sigma_\epsilon^2, \sigma_\eta^2|\boldsymbol{Y}) \tag{7}$$

Thus, to generate Monte Carlo samples of $\boldsymbol{Y}_{T+1}, \ldots, \boldsymbol{Y}_{T+\Delta T}$ from $p(\boldsymbol{Y}_{T+1}, \ldots, \boldsymbol{Y}_{T+\Delta T}|\boldsymbol{Y})$, we first generate parameters $\boldsymbol{u}_T, \boldsymbol{\theta}, D, w_x, w_y, \sigma_\epsilon^2$, and σ_η^2 from their posterior according to Equation (6) and then sample $\boldsymbol{u}_{T+1}, \ldots, \boldsymbol{u}_{T+\Delta T}$ in turn according to their transition probabilities. Assume $\nu_{i,T+\Delta t} = \text{logit}(p_{i,T+\Delta t})$ for $i = 1, \ldots, n$ and $\Delta t = 1, \ldots, \Delta T$. Then we sample $\boldsymbol{\nu}_{T+\Delta t}$ from $p(\boldsymbol{\nu}_{T+\Delta t}|\boldsymbol{\theta}, \boldsymbol{u}_{T+\Delta t}, \sigma_\epsilon^2)$ and let $p_{i,T+\Delta t} = \exp(\nu_{i,T+\Delta t})/\{1 + \exp(\nu_{i,T+\Delta t})\}$. Finally, we generate a sample of $Y_{i,T+\Delta t}$ from its posterior predictive distribution by simply drawing a random sample from its conditional distribution $p(Y_{i,T+\Delta t}|p_{i,T+\Delta t})$.

4. NUMERICAL EXAMPLE

4.1. Simulation study

A simulation study is conducted to study the capability of the model to capture different degrees of spatial–temporal dependence. We consider a 1×20 one-dimensional spatial lattice at 50 time points. To simulate the data, we assume that the logit of the probability of presence at time point t is $\text{logit}(\boldsymbol{p}_t) = \theta + \boldsymbol{u}_t + \boldsymbol{\epsilon}_t$ with $\theta = 1$ and variance parameters $\sigma_\epsilon^2 = \sigma_\eta^2 = 1$. We vary the diffusion rate D and convection rate w_x and w_y to obtain different diffusion–convection structure. Table 1 shows the posterior summary of the simulation study and Figure 3 compares the simulated $\boldsymbol{\nu}_t$ with posterior mean of $\boldsymbol{\nu}_t$. The results suggest that the proposed method captures different diffusion–convection structure very well.

In the simulation study, we also study different spatial structure for the residual $\boldsymbol{\eta}_t$ in the dynamic model. For example, a CAR model based on a pre-specified neighborhood structure or a variogram model is a possible choice. The simulation result shows that this small-scale spatial variation is not as easy to capture possibly due to the lack of information in binary data. However, this is not concerning, as $\boldsymbol{\eta}_t$ plays a minor role in trend estimation and prediction.

4.2. Mountain pine beetle outbreak example

We construct a spatial–temporal GLMM for the outbreak of MPB on the Chilcotin Plateau. We use the first 13 years of data from 1972 to 1984 for model fitting and reserve the last 2 years of data in 1985 and 1986 for model validation. We use noninformative priors for model parameters. The priors for the regression coefficients and diffusion–convection rates are assumed to be $N(0, 100)$. The prior for σ_η^2 is IG(2, 0.4) and the prior for σ_ϵ^2 is IG(2, 2). The Gibbs sampler was run for 20 000 iterations with

Table 1. The posterior mean and 95% credible bands for the models parameters in the simulation study

Parameter	True	Mean	True	Mean
D	0.3	0.294 (0.276, 0.312)	0.5	0.474 (0.463, 0.494)
w_x	0.2	0.206 (0.161, 0.259)	0	0.012 (−0.027, 0.054)
θ	1	0.997 (0.995, 1.004)	1	1.006 (0.974, 1.077)

DOI: 10.1002/env

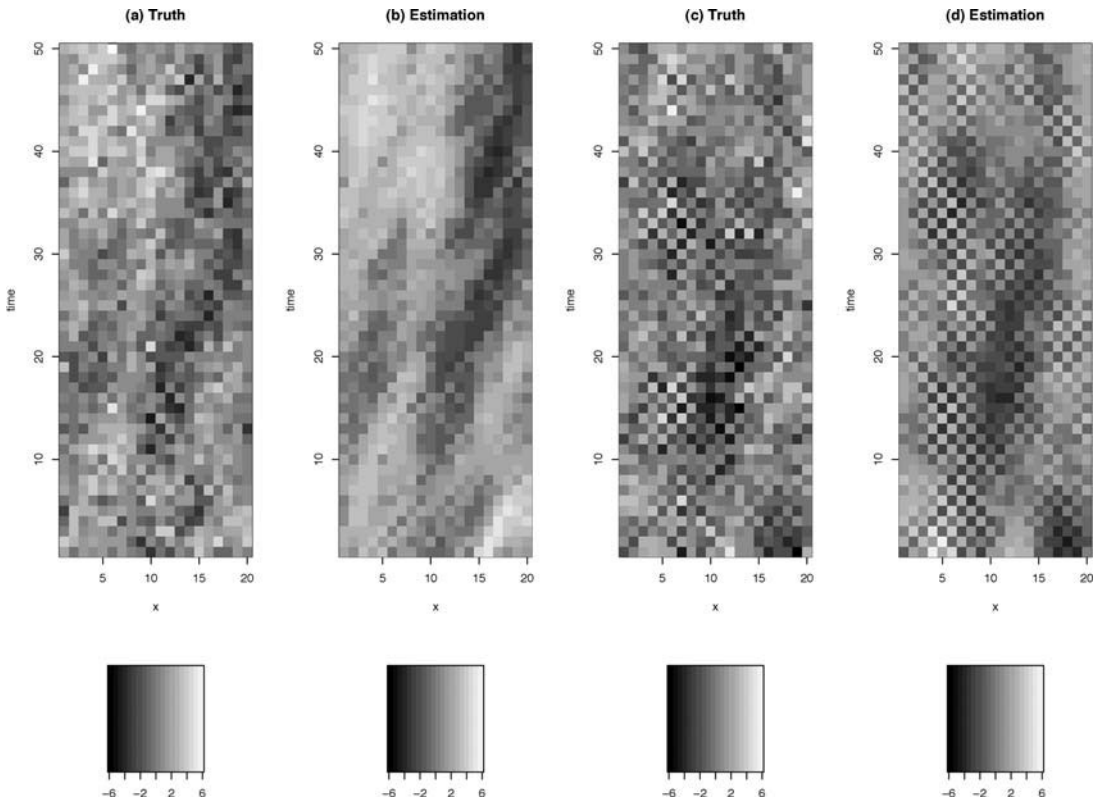

Figure 3. Simulated diffusion data and its posterior estimation: (a) Simulated $\boldsymbol{v}_t$ when $D = 0.3$ and $w_x = 0.2$; (b) Posterior mean for $\boldsymbol{v}_t$ when $D = 0.3$ and $w_x = 0.2$; (c) Simulated $\boldsymbol{v}_t$ when $D = 0.5$ and $w_x = 0$; (d) Posterior mean for $\boldsymbol{v}_t$ when $D = 0.5$ and $w_x = 0$

a burn-in length of 2000 to allow convergence of the chain. Every 20th of the Monte Carlo samples were saved to form an approximately independent Monte Carlo sample of size 1000. Figure 4 shows histograms of posteriors of the model parameters.

The performance of the model here is compared with the spatial–temporal autologistic regression model in Zhu *et al*. (2008). Table 2 shows the posterior summary of the parameters under the dynamic model and the maximum likelihood estimates of parameters for the autologistic model. Based on the dynamic model, there is some evidence of a negative relationship between MPB outbreak and elevation as well as number of days below -40°C, which is consistent with our prior knowledge that exposure to -40° is lethal to beetles and the regions with higher elevation are associated with less pine. This result is also consistent with the autologistic model. But the two models show different results for the relationship between MPB outbreak and mean August temperature. This could be due to the multicollinearity of the covariates. For the dynamic model, the diffusion rate is significantly positive but the convection rates are relatively small. This suggests that diffusion is the more important factor in the dispersal of the beetles. Since diffusion rate and convection rates are the parameters in the transition matrix, the significance of the diffusion rate and convection rates suggests the significance of the dynamics of $\boldsymbol{u}_t$. This is also

DOI: 10.1002/env

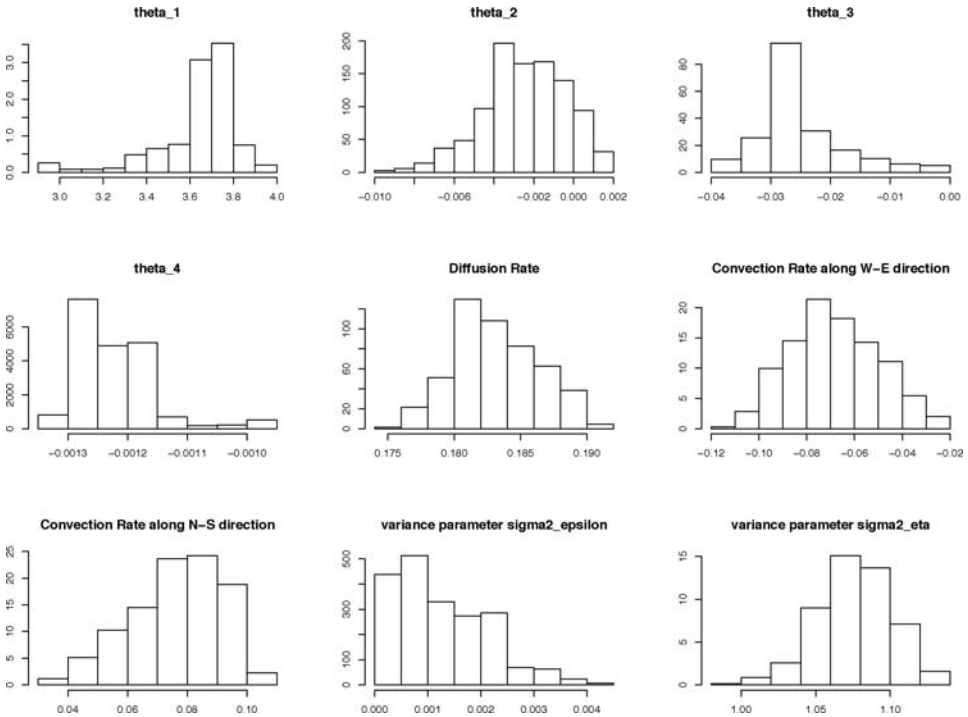

Figure 4. Histogram of Posterior samples

consistent with the autologistic model, which shows significant spatial and temporal correlation. The map of posterior latent process in Figure 5 shows a clear diffusion pattern, which agrees with the pattern of outbreak shown in Figure 2. This suggests that the latent process captures the dynamics of outbreak well.

Table 2. The posterior mean and 95% credible band for the models parameters based on the Monte Carlo samples generated from the posterior distribution. The MLEs and 95% confidence intervals for the parameters from the autologistic regression model (Zhu *et al*., 2008) are also provided for comparison

Term	Parameter	GLMM	Autologistic
Intercept	θ_0	3.639 (3.003, 3.887)	−3.35 (−3.76, −2.94)
X_1 Cold days	θ_1	−0.002 (−0.006, 0.001)	−0.013 (−0.027, 0.001)
X_2 August temp	θ_2	−0.025 (−0.036, −0.005)	0.019 (0.006, 0.033)
X_3 Elevation	θ_3	−0.0012 (−0.0013, −0.0010)	−0.0002 (−0.0003,−0.0001)
Diffusion coefficient	D	0.183 (0.177, 0.190)	
Convection coefficient	w_x	−0.068 (−0.100, −0.031)	
Convection coefficient	w_y	0.076 (0.045, 0.100)	
Spatial (first-order neighbor)			1.45 (0.71, 2.19)
Temporal 1-year lag			0.75 (0.61, 0.89)
Temporal 2-year lag			0.47 (0.31, 0.63)
Prediction error rate for 1985		0.30	0.29
Prediction error rate for 1986		0.54	0.56

DOI: 10.1002/env

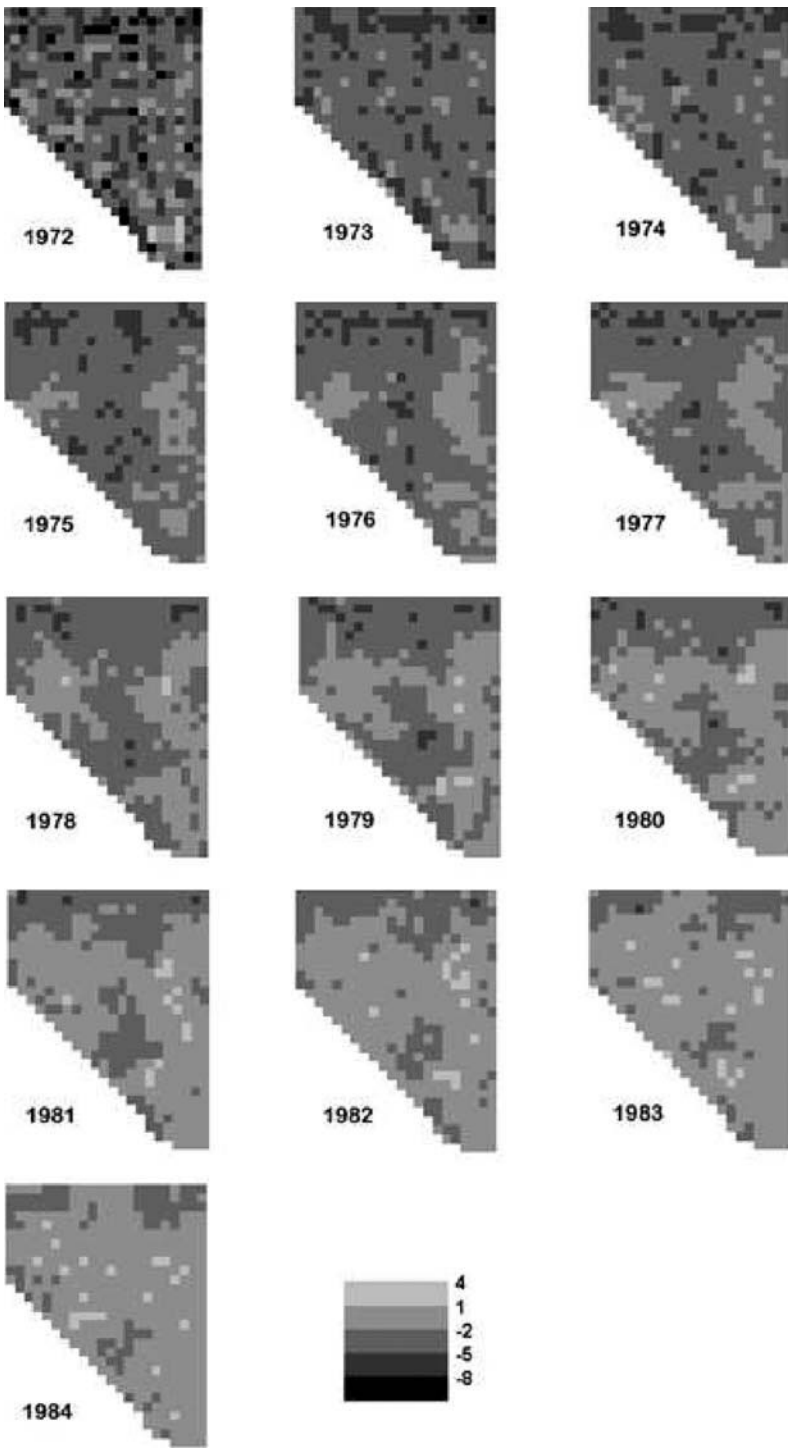

Figure 5. Maps of posterior mean of latent process from 1972 to 1984

DOI: 10.1002/env

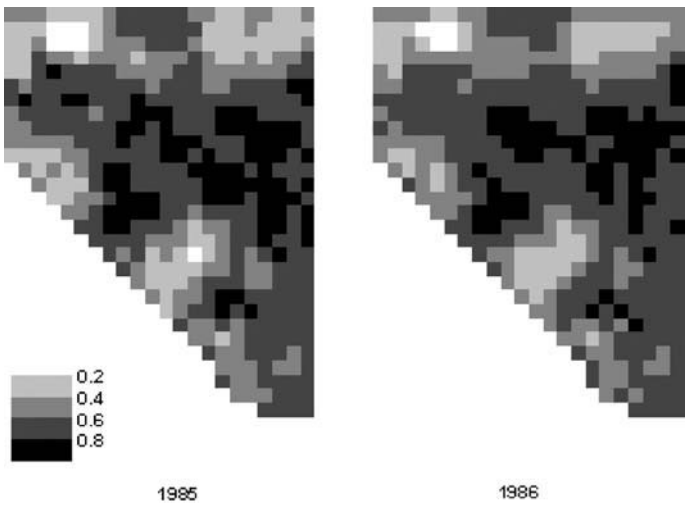

Figure 6. Maps of predicted risk of mountain pine beetle outbreak in 1985 and 1986

For model validation, we predict the outbreaks in 1985 and 1986. For each Monte Carlo sample of the model parameters, we generate one sample of $\boldsymbol{Y}_{T+1}$, $\boldsymbol{Y}_{T+2}$ from its posterior predictive distribution. Thus, we have a Monte Carlo sample of $\boldsymbol{Y}_{T+1}$, $\boldsymbol{Y}_{T+2}$ with sample size 1000. For each cell and time point, the mean of the Monte Carlo sample is computed and rounded to the nearest integer to predict whether that cell has an outbreak for that year. A prediction error rate is computed as the proportion of cells that are predicted differently from the actual observation. The prediction error rates are 0.30 and 0.54 for 1985 and 1986, respectively, which is comparable to the prediction errors for the autologistic model. Figure 6 shows the predicted risk of MPB outbreaks. The prediction error rate for 1985 is satisfying while for 1986 is quite high. The map of outbreak (Figure 2) shows that MPB population died off quickly after 1984. According to Stahl *et al*. (2006), the autumns in 1984 and 1985 were unusually cold, which led to the collapse of MPB populations. The lack of this information in the model is a possible reason for the high prediction error rate for 1986.

5. DISCUSSION

Here, we have developed a generalized linear mixed model for spatial–temporal binary data. We have applied the methodology to analyze a data set relating to MPB outbreaks on the Chilcotin Plateau in British Columbia, Canada. In the logit link function for the spatial–temporal GLMM, a regression is used to identify the effect of the environmental factors on MPB outbreaks and a latent dynamic process is used to account for spatial–temporal dependence. We have developed the statistical inference based on a Bayesian hierarchical modeling framework.

Although we have considered constant diffusion rate and convection rates, they can be extended to vary spatially (e.g., Wikle and Hooten, 2006) or temporally (e.g., Banks *et al*., 1988). In our model, we incorporate the effect of environmental factors directly into the modeling of spatial–temporal process $\boldsymbol{p}_t$. An alternative approach is to consider spatially- and temporally-varying diffusion rates and incorporate them into the diffusion model. Regarding the dynamics structure, we use a diffusion–convection PDE

DOI: 10.1002/env

model to describe the dynamics of the outbreak. The modeling framework developed can be used for different types of PDE dynamics. For example, a reaction–diffusion model can be applied if insects' movement is combined with population dynamics and multispecies interactions.

ACKNOWLEDGEMENTS

The authors acknowledge University of Kentucky and the Mountain Pine Beetle Initiative 7.05 of Natural Resources Canada for providing funding for this research. The authors would like to thank the editor and two reviewers for helpful comments and suggestions.

REFERENCES

Aukema BH, Carroll AL, Zheng Y, Zhu J, Raffa KF, Moore D, Stahl KK, Taylor SH. 2008. Movement of outbreak populations of mountain pine beetle: influences of spatiotemporal patterns and climate. *Ecography* **31**: 348–358.

Banerjee S, Carlin BP, Gelfand AE. 2004. *Hierarchical Modeling and Analysis for Spatial Data*. Chapman & Hall/CRC: Boca Raton, Florida.

Banks HT, Kareiva PM, Zia L. 1988. Analyzing field studies of insect dispersal using two–dimensional transport equations. *Environmental Entomology* **17**: 815–820.

Berliner LM. 1996. Hierarchical Bayesian time series models. In *Maximum Entropy and Bayesian Methods*, Hanson KM, Silver RN (eds). Kluwer: Dordrecht; 15–22.

Campbell EM, Alfaro RI, Hawkes B. 2007. Spatial distribution of mountain pine beetle outbreaks in relation to climate and stand characteristics: a dendroecological analysis. *Journal of Integrative Plant Biology* **49**: 168–178.

Clark JS. 2007. *Models for Ecological Data: An Introduction*. Princeton University Press: New Jersey.

Cressie N, Huang HC. 1999. Classes of nonseparable, spatio–temporal stationary covariance functions. *Journal of the American Statistical Association* **94**: 1330–1340.

de la Giroday HM. 2009. Spatial associations between infestations of mountain pine beetle and landscape features in the Peace River region of British Columbia. *M.Sc. Thesis*, Natural Resources and Environmental Studies, University of Northern British Columbia, Prince George, British Columbia, Canada. 120 pp.

Diggle PJ, Tawn JA, Moyeed RA. 1998. Model-based geostatistics. *Applied Statistics* **47**: 453–473.

Gneiting T. 2002. Nonseparable, stationary covariance functions for space-time data. *Journal of the American Statistical Association* **97**: 590–600.

Haberman R. 1987. *Elementary Applied Partial Differential Equations* (2nd edn). Prentice-Hall: New Jersey.

Holmes EE, Lewis MA, Banks JE, Veit RR. 1994. Partial differential equations in ecology: spatial interactions and population dynamics. *Ecology* **75**: 17–29.

Hooten MB, Wikle CK. 2007. Invasions, epidemics, and binary data in a cellular world. *Proceedings of the American Statistical Association* [CD-ROM]. American Statistical Association: Alexandria, VA; 3999–4010.

Hooten MB, Wikle CK. 2008. A hierarchical Bayesian non–linear spatio–temporal model for the spread of invasive species with application to the Eurasian Collared-Dove. *Environmental and Ecological Statistics* **15**: 59–70.

Jackson PL, Straussfogel D, Lindgren BS, Mitchell S, Murphy B. 2008. Radar observation and aerial capture of mountain pine beetle, Dendroctonus ponderosae Hopk. (Coleoptera: Scolytidae) in flight above the forest canopy. *Canadian Journal of Forest Research-Revue Canadienne De Recherche Forestiere* **38**: 2313–2327.

Kurz WA, Dymond CC, Stinson G, Rampley GJ, Neilson ET, Carroll A, Ebata T, Safranyik L. 2008. Mountain pine beetle and forest carbon feedback to climate change. *Nature* **452**: 987–990.

McCullagh P, Nelder JA. 1989. *Generalized Linear Models* (2nd edn). Chapman & Hall: Boca Raton.

Okubo A, Levin SA. 2001. *Diffusion and Ecological Problems: Modern Perspectives*. Spring-Veleg: New York.

Powell JA, Jenkins JL, Logan JA, Bentz BJ. 2000. Seasonal temperature alone can synchronize life cycles. *Bulletin of Mathematical Biology* **62**: 977–998.

Raffa KF, Aukema BH, Bentz BJ, Carroll AL, Hicke JA, Turner MG, Romme WH. 2008. Cross–scale drivers of natural disturbances prone to anthropogenic amplification: the dynamics of bark beetle eruptions. *BioScience* **58**: 501–517.

Royle JA, Dorazio RM. 2008. *Hierarchical Modeling and Inference in Ecology: The Analysis of Data from Populations, Metapopulations and Communities*. Elsevier: London.

Safranyik L, Linton DA, Silversides R, Mcmullen LH. 1992. Dispersal of released mountain pine beetles under the canopy of a mature lodgepole pine stand. *Journal of Applied Entomology-Zeitschrift Fur Angewandte Entomologie* **113**: 441–450.

Safranyik L, Shrimpton DM, Whitney HS. 1975. An interpretation of the interaction between lodgepole pine, the mountain pine beetle and its associated blue stain fungi in Western Canada. In *Management of Lodgepole Pine Ecosystems Symposium*

DOI: 10.1002/env

Proceedings, Baumgartner DM (ed.). Washington State University Cooperative Extension Service: Pullman, Washington; 406–428.

Stahl K, Moore RD, McKendry IG. 2006. Climatology of winter cold spells in relation to mountain pine beetle mortality in British Columbia, Canada. *Climate Research* **32**: 13–23.

Wikle CK. 2003. Hierarchical Bayesian models for predicting the spread of eological processes. *Ecology* **84**: 1382–1394.

Wikle CK, Hooten MB. 2006. Hierarchical Bayesian spatio–temporal models for population spread. In *Applications of Computational Statistics in the Environmental Sciences: Hierarchical Bayes and MCMC Methods*, Clark JS, Gelfand AE (eds). Oxford University Press: Oxford.

Wikle CK, Milliff RF, Nychka D, Berliner LM. 2001. Spatial–temporal hierarchical Bayesian modeling. *Journal of the American Statistical Association* **96**: 382–397.

Wygant ND. 1940. Effects of low temperature on the black hills beetle (Dendroctonus ponderosae Hopk.). In *Summary of Ph.D. Thesis Submitted to New York School of Forestry*, on File at USDA Rocky Mountain Forest and Range Experiment Station, Fort Collins, Colorado; 57, 16 Figs.

Zhu J, Huang HC, Wu J. 2005. Modeling spatial-temporal binary data using Markov Random Model. *Journal of Agricultural, Biological, and Environmental Statistics* **10**: 212–225.

Zhu J, Zheng Y, Carroll AL, Aukema BH. 2008. Autologistic regression analysis of spatial–temporal binary data via Monte Carlo maximum likelihood. *Journal of Agricultural, Biological, and Environmental Statistics* **13**: 84–98.

APPENDIX: FULL CONDITIONAL DISTRIBUTIONS

- $[\text{logit}(p_{i,t})|\cdot]$. Let $\nu_{i,t} = \text{logit}(p_{it})$ for notational convenience. For $i = 1, \ldots, n$ and $t = 1, \ldots, T$, we sample from its full-conditional by utilizing an MH algorithm:

  1. Generate $\nu_{i,t}^* \sim N\left(\nu_{i,t}^{(j-1)}, \sigma_\nu^2\right)$ and compute the ratio,

$$r = \frac{\left[Y_{i,t}|\nu_{i,t}^*\right]\left[\nu_{i,t}^*|\boldsymbol{\theta}^{(j-1)}, \boldsymbol{u}_t^{(j-1)}, \sigma_\epsilon^{2,(j-1)}\right]}{\left[Y_{i,t}|\nu_{i,t}^{(j-1)}\right]\left[\nu_{i,t}^{(j-1)}|\boldsymbol{\theta}^{(j-1)}, \boldsymbol{u}_t^{(j-1)}, \sigma_\epsilon^{2,(j-1)}\right]}$$

  2. Set $\nu_{i,t}^{(j)} = \nu_{i,t}^*$ with probability $\min(r, 1)$. Otherwise, set $\nu_{i,t}^{(j)} = \nu_{i,t}^{(j-1)}$.

- $[\boldsymbol{u}_0|\cdot]$. Prior $\boldsymbol{u}_0 \sim N(\boldsymbol{\mu}_0, \boldsymbol{\Sigma}_0)$. Let $\boldsymbol{\Sigma} = \sigma_\eta^2 \boldsymbol{I}$. Sample from $\boldsymbol{u}_0^{(j)} \sim N(\boldsymbol{Ab}, \boldsymbol{A})$ where

$$\boldsymbol{A} = \left(\boldsymbol{H}'^{(j-1)}(\boldsymbol{\Sigma}^{(j-1)})^{-1}\boldsymbol{H}^{(j-1)} + \boldsymbol{\Sigma}_0^{-1}\right)^{-1},$$
$$\boldsymbol{b} = \boldsymbol{\Sigma}_0^{-1}\boldsymbol{\mu}_0 + \boldsymbol{H}'^{(j-1)}\left(\boldsymbol{\Sigma}^{(j-1)}\right)^{-1}\boldsymbol{u}_1^{(j-1)}$$

- $[\boldsymbol{u}_t|\cdot]$ for $t = 1, \ldots, T-1$. Sample from $\boldsymbol{u}_t^{(j)} \sim N(\boldsymbol{Ab}, \boldsymbol{A})$ where

$$\boldsymbol{A} = \left((\boldsymbol{\Sigma}^{(j-1)})^{-1} + \boldsymbol{H}'^{(j-1)}(\boldsymbol{\Sigma}^{(j-1)})^{-1}\boldsymbol{H}^{(j-1)} + \boldsymbol{I}/\sigma_\epsilon^{2,(j-1)}\right)^{-1},$$
$$\boldsymbol{b} = \boldsymbol{H}'^{(j-1)}(\boldsymbol{\Sigma}^{(j-1)})^{-1}\boldsymbol{u}_{t+1}^{(j-1)} + (\boldsymbol{\Sigma}^{(j-1)})^{-1}\boldsymbol{H}^{(j-1)}\boldsymbol{u}_{t-1}^{(j)} + \left(\boldsymbol{v}_t^{(j)} - \boldsymbol{X}_t\boldsymbol{\theta}^{(j-1)}\right)/\sigma_\epsilon^{2,(j-1)}$$

  where $\boldsymbol{X}_t = (\boldsymbol{X}_{1,t}, \ldots, \boldsymbol{X}_{K,t})$ and $\boldsymbol{v}_t = (\nu_{1,t}, \ldots, \nu_{n,t})'$.

- $[\boldsymbol{u}_T|\cdot]$. Sample from $\boldsymbol{u}_T^{(j)} \sim N(\boldsymbol{Ab}, \boldsymbol{A})$ where

$$\boldsymbol{A} = \left(\boldsymbol{\Sigma}^{(j-1)} + \boldsymbol{I}/\sigma_\epsilon^{2,(j-1)}\right)^{-1},$$
$$\boldsymbol{b} = (\boldsymbol{\Sigma}^{(j-1)})^{-1}\boldsymbol{H}^{(j-1)}\boldsymbol{u}_{T-1}^{(j)} + \left(\boldsymbol{v}_T^{(j)} - \boldsymbol{X}_T\boldsymbol{\theta}^{(j-1)}\right)/\sigma_\epsilon^{2,(j-1)}$$

DOI: 10.1002/env

- $[\boldsymbol{\theta}|\cdot]$. Prior $\boldsymbol{\theta} \sim N(\boldsymbol{\theta}_0, \Sigma_{\theta_0})$. Sample from $\boldsymbol{\theta}^{(j)} \sim N(\boldsymbol{Ab}, \boldsymbol{A})$ where

$$\boldsymbol{A} = \left(\boldsymbol{\Sigma}_{\theta_0}^{-1} + \boldsymbol{X}'\boldsymbol{X}/\sigma_\epsilon^{2,(j-1)}\right)^{-1},$$
$$\boldsymbol{b} = \boldsymbol{X}'\left(\boldsymbol{v}^{(j)} - \boldsymbol{u}^{(j)}\right)/\sigma_\epsilon^{2,(j-1)} + \boldsymbol{\Sigma}_{\theta_0}^{-1}\boldsymbol{\theta}_0$$

  where $\boldsymbol{X} = (\boldsymbol{X}_1', \ldots, \boldsymbol{X}_T')'$, $\boldsymbol{v} = (\boldsymbol{v}_1', \ldots, \boldsymbol{v}_T')'$, and $\boldsymbol{u} = (\boldsymbol{u}_1', \ldots, \boldsymbol{u}_T')'$.
- $[D|\cdot]$. Prior $D \sim N(\mu_D, \sigma_D^2)$. Rewrite (5) as

$$\boldsymbol{u}_t = \boldsymbol{u}_{t-1} + D\boldsymbol{B}_{t-1;1} + w_x\boldsymbol{B}_{t-1;2} + w_y\boldsymbol{B}_{t-1;3} + \boldsymbol{\eta}_t$$

  where $\boldsymbol{B}_{t-1;1}$, $\boldsymbol{B}_{t-1;2}$, and $\boldsymbol{B}_{t-1;3}$ are vectors of functions of $\boldsymbol{u}_{t-1}$. Sample from $D^{(j)} \sim N(ab, a)$ where

$$a = \left(\sum_{t=1}^{T} \boldsymbol{B}_{t-1;1}'^{(j)}(\boldsymbol{\Sigma}^{(j-1)})^{-1}\boldsymbol{B}_{t-1;1}^{(j)} + 1/\sigma_D^2\right)^{-1},$$
$$b = \sum_{t=1}^{T} \boldsymbol{B}_{t-1;1}'^{(j)}(\boldsymbol{\Sigma}^{(j-1)})^{-1}\left(\boldsymbol{u}_t^{(j)} - \boldsymbol{u}_{t-1}^{(j)} - w_x\boldsymbol{B}_{t-1;2}^{(j)} - w_y\boldsymbol{B}_{t-1;3}^{(j)}\right) + \mu_D/\sigma_D^2$$

- $[w_x|\cdot]$. Prior $w_x \sim N(\mu_x, \sigma_x^2)$. Sample from $w_x^{(j)} \sim N(ab, a)$ where

$$a = \left(\sum_{t=1}^{T} \boldsymbol{B}_{t-1;2}'^{(j)}(\boldsymbol{\Sigma}^{(j-1)})^{-1}\boldsymbol{B}_{t-1;2}^{(j)} + 1/\sigma_x^2\right)^{-1},$$
$$b = \sum_{t=1}^{T} \boldsymbol{B}_{t-1;2}'^{(j)}(\boldsymbol{\Sigma}^{(j-1)})^{-1}\left(\boldsymbol{u}_t^{(j)} - \boldsymbol{u}_{t-1}^{(j)} - D\boldsymbol{B}_{t-1;1}^{(j)} - w_y\boldsymbol{B}_{t-1;3}^{(j)}\right) + \mu_x/\sigma_x^2$$

- $[w_y|\cdot]$. Prior $w_y \sim N(\mu_y, \sigma_y^2)$. Sample from $w_y^{(j)} \sim N(ab, a)$ where

$$a = \left(\sum_{t=1}^{T} \boldsymbol{B}_{t-1;3}'^{(j)}(\boldsymbol{\Sigma}^{(j-1)})^{-1}\boldsymbol{B}_{t-1;3}^{(j)} + 1/\sigma_y^2\right)^{-1},$$
$$b = \sum_{t=1}^{T} \boldsymbol{B}_{t-1;3}'^{(j)}(\boldsymbol{\Sigma}^{(j-1)})^{-1}\left(\boldsymbol{u}_t^{(j)} - \boldsymbol{u}_{t-1}^{(j)} - D\boldsymbol{B}_{t-1;1}^{(j)} - w_x\boldsymbol{B}_{t-1;2}^{(j)}\right) + \mu_y/\sigma_y^2$$

- $[\sigma_\epsilon^2|\cdot]$. Prior $IG(\alpha_\epsilon, \gamma_\epsilon)$. Sample from $IG(\alpha, \gamma)$ where

$$\alpha = \alpha_\epsilon + nT/2,$$
$$\gamma = \left(1/\gamma_\epsilon + \frac{1}{2}\sum_{t=1}^{T}\left(\boldsymbol{v}_t^{(j)} - \boldsymbol{X}_t\boldsymbol{\theta}^{(j)} - \boldsymbol{u}_t^{(j)}\right)'\left(\boldsymbol{v}_t^{(j)} - \boldsymbol{X}_t\boldsymbol{\theta}^{(j)} - \boldsymbol{u}_t^{(j)}\right)\right)^{-1}$$

DOI: 10.1002/env

- $[\sigma_\eta^2|\cdot]$. Prior $IG(\alpha_\eta, \gamma_\eta)$. Sample from $IG(\alpha, \gamma)$ where

$$\alpha = \alpha_\eta + nT/2,$$
$$\gamma = \left(1/\gamma_\eta + \frac{1}{2}\sum_{t=1}^{T}\left(\boldsymbol{u}_t^{(j)} - \boldsymbol{H}^{(j)}\boldsymbol{u}_{t-1}^{(j)}\right)'\left(\boldsymbol{u}_t^{(j)} - \boldsymbol{H}^{(j)}\boldsymbol{u}_{t-1}^{(j)}\right)\right)^{-1}$$

DOI: 10.1002/env